# Effect of PEM Fuel Cell Exhaust Water Conductivity on Catalyst Degradation using Thermal Degradation Resistant Polymer Membranes

**Theodore. E. Burye**[a]

[a] *U.S. Army Ground Vehicles Systems Center, 6501 E Eleven Mile Rd, MS 121, Warren, MI 48397, USA, Theodore.e.burye2.civ@mail.mil*

Here, energy dispersive spectroscopy, X-ray diffraction and Williamston-Hall particle size and strain characterization are used to determine the effect of solution conductivity, heating and electrical current on Proton Exchange Membrane electrocatalyst degradation and its underlying mechanism. Quartz containing polybenzimidazole polymer samples are sputter-coated with 6nm thick layers of platinum while 100 to 400 current cycles are applied. 100 cycles of 0.7mA current removes 38% of the platinum coating while also in contact with a water containing 5 vol% acetic acid. This data suggests a possible mechanism involves the transportation of quartz to the polymer surface which combines with the platinum. The interaction between quartz and platinum increases quartz's lattice strain to 1.4% and results in quartz and platinum detaching. Thermal decomposition of polymer membranes, which contain additives (such as acid side chains), could change the properties of water produced and increase its electrical conductivity thus promoting stack degradation.

**Keywords:** Proton Exchange Membrane; Hydrogen; Fuel Cells; Degradation; Thermally Resistant Polymers; Catalysts

## 1. Introduction

Proton Exchange Membrane Fuel Cells (PEMFCs) are clean energy producing devices which offer increased chemical to electric conversion efficiencies, low temperature operation, and produce water as a byproduct. These advantages have promoted PEMFC devices as possible alternatives to provide power in place of conventional internal combustion (IC) engines for stationary and transportation applications. As the PEMFC device technology is advanced and implemented into applications which traditionally used IC engines, these devices are expected to have comparable performance and durability demonstrated by IC engines. Unfortunately, there are many different degradation mechanisms in low-temperature PEMFCs [1-4] which lower stack performance and durability and hinder PEMFCs from being accepted as a viable power generating alternative.

Degradation mechanisms which impact the electrocatalyst material and electrocatalyst support structure (such as the polymer membrane) can be especially damaging to the stack and can be caused by many different operating parameters including temperature [5-11], humidity and oxygen partial pressure [6-9, 11-18], electrical bias cycles and continuous operation [2, 10, 15, 17, 19-22], cell potential [16], catalyst particle size [9, 23], catalyst poisoning [14] and solution chemistry [1, 2] to name some of the more common parameters.

Many of these different parameters have been investigated extensively and potential solutions have been determined, which mitigate some of these problems. Some mitigation strategies include the incorporation of silicon into the polymer membrane which increases polymer thermal degradation resistance [24-27], increases polymer mechanical strength and improves polymer hydration [25, 28].

Despite these advancements, the effect of changes to the PEM exhaust water chemistry on electrocatalyst degradation needs to be examined further. Gilbert *et al.* [2] and Shao-Horn *et al.* [1] have shown that

platinum catalyst, coated onto a polymer membrane, can be removed when in contact with an acidic solution when an electrical bias/current was applied. Both authors demonstrate the impact an electrical bias/current can potentially have on the amount of platinum dissolved into the acidic solution, but neither go into detail to explain the effect the solution had on, or the mechanism behind, the platinum degradation in the cell.

Gilbert *et al.* conducted experiments using perchloric acid, which is a weak acid. Weak acid solutions have the capability of conducting electrons which potentially may increase the catalyst degradation rate. This potential degradation process is important to understand for the following reasons:

1. Water, a natural byproduct of PEMFCs, can become weakly acidic over time when stagnant, which could potentially occur when the fuel cell is stored between operation in transportation applications.
2. Depending on the additives [10, 27, 29] applied to the PEMFC cell membrane material, thermal decomposition of the membrane material during operation potentially could change solution properties. Some of these additives are acid side chains [10, 27, 30], including acetic acid, which potentially could contribute to the acidification of the water.

Due to a possible connection between solution conductivity and catalysis degradation, the objective of this work was to characterize the impact changes in the solution conductivity, produced by the PEMFC, on the rate of catalyst loss from the fuel cell as a function of electrical current cycles.

## 2. Material and methods

The experimental setup outlined in this paper investigates the nanoscale region where the electrocatalyst material, polymer membrane substrate and solution (water) (produced by the fuel cell) make contact with each other within the cathode electrode inside a PEM fuel cell. The electrocatalyst material used in PEM fuel cells are typically manufactured as nano-sized particles [31, 32] and are capable of conducting an electrical current to complete the half-reactions in each electrode. In addition, as previously mentioned, thermal degradation of the polymer substrate, near the surface, can change the properties of the water produced through the electrochemical reaction. Some property changes to the water produced by the fuel cell, as mentioned, have been report by Gilbert *et al.* [2] and Shao-Horn *et al.* [1] to degrade the catalyst material when in contact with the catalyst at the polymer substrate interface. Quartz nanoparticles were incorporated into the polymer to be consistent with previous literature studies which used quartz to improve thermal degradation resistance in their fuel cell polymer membranes [24-27, 33]. Many of these studies combined both acid side chains (which can leach and alter water chemistry) and quartz/silica into their polymer membranes [24, 26, 33] which this study replicated to account for all possible variables if acid side chains were leached into the exhaust water.

In addition to simulating the interaction between the electrocatalyst material, polymer substrate and solution the experimental conditions used in this study did not use oxygen or hydrogen gasses to generate an electrical current through the catalyst material so as to focus on the interaction between these three elements. To simulate the electrical current generated within a PEM fuel cell from the electrochemical half-reactions between oxygen and hydrogen an external power supply was used. The catalyst nanoparticles used in a PEM fuel cell were approximated by an electrically interconnected nano-sized sputter-coating of platinum particles across the surface of a polymer substrate. These substitutions are considered reasonable approximations of the interior structure within the PEM fuel cell to investigate the effect of the solution when in contact with the catalyst material and the polymer substrate.

Using the experimental setup outlined above, the underlying mechanism behind PEM fuel cell catalyst degradation was investigated. Samples were characterized using different heating conditions, PEM solution chemistries, and/or potentiodynamic (cycling) conditions to determine which parameters would degrade/remove the platinum layer.

*Catalyst-membrane sample production*

Samples preparation was started by using a Polybenzimidazole (PBI) polymer membrane containing a homogeneous distribution of 6nm size quartz particles, which was prepared via proprietary methods. All polymer samples were 70µm in thickness and had a ¼ $in^2$ surface area.

Platinum catalyst was then sputter-coated (Quorum; Laughton, East Sussex, United Kingdom), using a 99.99% pure platinum target (Electron Microscopy Sciences; Hatfield, PA, USA) with a 57mm diameter and 100µm thickness. Platinum sputter-coatings were applied to a single side of each polymer membrane sample with a thickness of 6nm. Depending

on the characterization test being performed the platinum sputter-coating was applied differently.

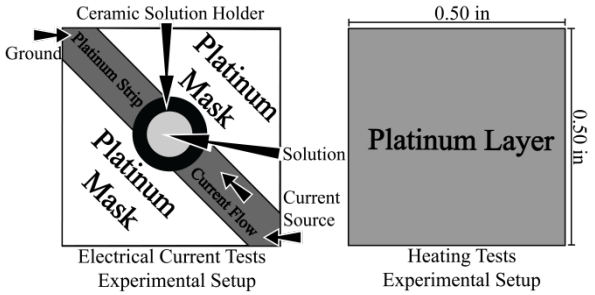


**Fig. 1.** Experimental setup for electrical current and heating tests. A polymer membrane with 0.25 $in^2$ surface area was sputter coated with 6nm of platinum electrocatalyst on one side. The coating was applied as a 0.635 cm long, 0.238 cm wide strip using masks with a ceramic holder (0.409 $cm^3$ volume) attached which contained the interaction solution for current cycle tests. The platinum coating was applied across the entire surface for heating experiments.

Polymer membrane samples used for characterizing heating parameters had the sputter-coating of platinum applied to the entire polymer membrane surface on one side, while samples used for characterizing electrical current parameters had the sputter-coating of platinum applied as a thin strip by applying a mask prior to the sputter-coating process, shown in Fig. 1. The resulting platinum strip for each sample was 0.635 cm in length and 0.238 cm in width. In addition, a ceramic holder, with a ¼ inch inside diameter and 0.409 $cm^3$ (0.409 mL) solution volume, was placed over the platinum in the center of each sample prior to testing.

*Heating and solution chemistry measurement experimental setup*

Platinum-coated polymer membrane samples were submerged in 10mL of solution inside glass beakers with the platinum coating facing upwards. Solutions used were: 1. 16 MΩ deionized water (DI water) (referred as 0 vol% acetic acid for the remainder of this paper), 2. 5 vol% acetic acid and, 3. glacial acetic acid (Fisher Scientific, Waltham, MA, USA) (referred to 99.7 vol% acetic acid for the remainder of this paper). Samples placed in solutions were heated using set points varying from 65-150°C for a total of 2,280 min (38 hrs) each, while at ambient pressure. As solutions evaporated during the heating process an additional 2-3mL of solution was added, when needed, to maintain the starting volume of 10mL. Three samples were tested, for each parameter being tested, to account for statistical variations in sample measurements.

*Potentiodynamic and solution chemistry measurement experimental setup*

Polymer membrane samples were prepared as shown in Fig. 1. The ceramic holder was filled with either 0 vol%, 5 vol% or 99.7 vol% acetic acid solution chemistries prior experimentation. Leads from a variable voltage/current power supply were connected to each side of the platinum strip with either a constant 0.7mA or 30mA current being applied across the platinum coating. Voltages across through the platinum surface were calculated, using the platinum resistivity from literature [34], and found to on average 2.6V and 0.06V, respectively. Currents were applied using a square wave profile with 5s/5s, where one square wave profile will be referred for the remainder of the paper as 1 cycle. Samples had 50, 100, 200 or 400 cycles applied which took 8 min, 17 min, 33 min and 67 min to complete, respectively. Three samples were also tested, for each parameter being tested as with the heating experiments.

*Energy Dispersive Spectroscopy (EDS) measurements*

Platinum and silicon elemental sample level measurements before and after experimentation were performed using a Hitachi Scanning Electron Microscope (SEM) (Hitachi; Krefeld, Germany) with an Oxford Instruments Energy Dispersive Spectroscopy (EDS) detector (Oxford Instruments; Concord, MA, USA). EDS measurements were taken using a beam voltage of 30.0 kV, a 30µm aperture, a 256 s scan speed, a 10mm working distance, and a 200x magnification. At least three EDS measurements were averaged for each sample, before and after experiments, to account for variations through the platinum coating.

EDS samples were prepared using two different approaches for heating and electrical current tests. Samples heated in different solutions were removed from their respective solution, allowed to air dry and then analyzed. Samples which had an electrical current applied while in contact with different solutions first had the ceramic solution holder removed, allowed to air dry then the platinum in contact with the solution was cut away and analyzed.

*X-ray Diffraction (XRD) measurements*

Polymer membrane and platinum coating particle structures were evaluated using X-ray diffraction (XRD). XRD characterizations were conducted at room temperature from $3° \leq 2\theta \leq 90°$ with a 0.010 step, a 2.00

s scan speed, a copper filament and nickel filter using a SmartLab (Rigaku Americas Corporation; The Woodlands, TX, USA) operated at 20 kV and 10 mA.

*Williamson-Hall particle size and strain calculations*

Quartz (contained within the polymer membrane samples) and platinum strain and/or particle sizes were calculated using the Williamson-Hall method [35]. The Split Pseudo-Voigt shape function using a Lorentz background was used to calculate the FWHM values for each peak using the PDXL Rigaku analysis software. Peak breadth (β) values were calculated using the FWHM values. Particle sizes were determined from the linear intercept, and strain values were determined from the slope from plots of βcos(θ) vs. 4sin(θ) using the Willamson-Hall method. The particle size was calculated using Equation 1 and the strain was determined from the slope of the plot:

$$\frac{K*\lambda}{intercept} = D \quad (1)$$

where *D* is the average quartz particle size in nm, *K* is the shape factor (0.9 used for calculations) and *λ* is the x-ray wavelength (0.154 nm for Cu $K_\alpha$ x-rays).

*Platinum sputter-coating current measurements and voltage calculations*

Current measurements and calculated voltages through coatings were conducted by first fabricating six platinum sputter-coated polymer membrane samples as shown in Fig. 1 (left illustration). Coating thicknesses were maintained at 6nm where lengths and widths were measured using a caliper for accuracy. Finally, the variable current/voltage power supply was connected to each end of the coating passing and average of ~28mA through the platinum. The resulting current was measured and recorded. Coating resistance values were calculated using Equation 2:

$$\frac{\rho*L}{A} = R \quad (2)$$

where *R* is the coating resistance in Ω, *ρ* is the platinum electrical resistivity in Ω*m from literature (value used was 10.6 * $10^{-8}$ Ω*m) [34], *A* is the cross sectional area of the platinum strip measured in $m^2$ and *L* is the length of the platinum strip measured in meters. Voltages through each coating were then calculated using Ohm's Law, the recorded current values and resistance values calculated using Equation 2. Both measured and calculated values are shown in Table 1.

## 3. Results

Table 2 shows the heating experimental conditions used and the initial platinum and silicon EDS results determined for each sample so only one variable was adjusted at a time. Polymer surface area was maintained at 0.25 $in^2$ to ensure consistency. Each solution volume was maintained at 10 mL during heating experiments and each solution was only allowed to decrease by 2-3 mL before additional solution was added to return to its initial volume. Solution volumes were maintained close to their initial volumes so that solution acid concentrations (specifically with the 5 vol% samples) did not change significantly with time.

Table 3 shows the electrical current cycle experimental conditions used and the initial platinum and silicon EDS results determined for each sample so only one variable was adjusted at a time. Both the polymer surface area and platinum coating areas were maintained to ensure consistency between samples. After each ceramic holder was attached its entire volume was filled with solution. Samples had between 50 and 400 cycles applied across the platinum coating using either a 0.7mA or 30mA electrical current.

### *3.1 The effect of heating and solution acidity concentration on platinum and silicon particle levels*

Platinum sputter-coated polymer membrane samples were heated to test whether applied heat in combination with different solution chemistries could result in platinum being removed.

Fig. 2 shows the platinum and silicon raw EDS peak intensity data from each platinum sputter-coated membrane sample before and after being heated using the experimental conditions shown in Table 2. Heating samples for 38 hrs did not appear to have much effect on the platinum peak intensities for any temperature or solution combination. The silicon peak intensities did show a marginal increase when using either the 0 vol% or 5 vol% acetic acid solution when heated using a 100°C or 150°C set point.

Fig. 3 shows the average and statistical variations in platinum and silicon peak heights calculated from the EDS raw data obtained from the three samples used for each adjusted parameter. Data trends were similar to the results in Fig. 2 except for two exceptions. The increase in silicon for all three 5 vol% acetic acid solution temperatures was not statistically significant and the 0 vol% 150°C set point solution showed a statistically marginal increase.

**Table 1**

Platinum sputter coating resistivity parameters

| Sample # | Coating Thickness (nm) | Measured Current through Coating (mA) | Platinum Sputter Coating Strip Cross Sectional Area ($m^2$) | Platinum Sputter Coating Strip Length (m) | Calculated Electrical Resistance Across Coating (Ω) | Calculated Voltage Across Coating (V) |
|---|---|---|---|---|---|---|
| 1P | 6.0 | 30 | $2.9 * 10^{-11}$ | 0.020 | 74.1 | 2.2 |
| 2P | 6.0 | 20 | $2.0 * 10^{-11}$ | 0.022 | 116.7 | 2.3 |
| 3P | 6.0 | 30 | $2.3 * 10^{-11}$ | 0.018 | 88.3 | 2.7 |
| 4P | 6.0 | 30 | $2.2 * 10^{-11}$ | 0.022 | 102.0 | 3.1 |
| 5P | 6.0 | 40 | $3.2 * 10^{-11}$ | 0.021 | 69.2 | 2.8 |
| 6P | 6.0 | 30 | $2.7 * 10^{-11}$ | 0.021 | 81.3 | 2.4 |

**Table 2**

Platinum sputter coating polymer membrane heating parameters

| Sample # | Platinum Coating Thickness (nm) | Solution Volume (mL) | Solution Heating Time (hr) | Solution Acetic Acid % (vol%) | Heating Temperature Set Point (°C) |
|---|---|---|---|---|---|
| 1H | 6.0 | 10 | 38 | 0 | 65 |
| 2H | 6.0 | 10 | 38 | 0 | 100 |
| 3H | 6.0 | 10 | 38 | 0 | 150 |
| 4H | 6.0 | 10 | 38 | 5 | 65 |
| 5H | 6.0 | 10 | 38 | 5 | 100 |
| 6H | 6.0 | 10 | 38 | 5 | 150 |
| 7H | 6.0 | 10 | 38 | 99.7 | 65 |
| 8H | 6.0 | 10 | 38 | 99.7 | 100 |
| 9H | 6.0 | 10 | 38 | 99.7 | 150 |

**Table 3**

Platinum sputter coating polymer membrane in contact with solution electrical current parameters, 30mA Current

| Sample # | Platinum Coating Thickness (nm) | Solution Volume (mL) | Solution Temperature (°C) | Applied Electrical Current (mA) | Solution Acetic Acid % (vol%) | # Current Cycles |
|---|---|---|---|---|---|---|
| 1E-30 | 6.0 | 0.409 | 21 | 30 | 0 | 100 |
| 2E-30 | 6.0 | 0.409 | 21 | 30 | 0 | 200 |
| 3E-30 | 6.0 | 0.409 | 21 | 30 | 0 | 400 |
| 4E-30 | 6.0 | 0.409 | 21 | 30 | 5 | 50 |
| 5E-30 | 6.0 | 0.409 | 21 | 30 | 5 | 100 |
| 6E-30 | 6.0 | 0.409 | 21 | 30 | 5 | 200 |
| 7E-30 | 6.0 | 0.409 | 21 | 30 | 99.7 | 100 |
| 8E-30 | 6.0 | 0.409 | 21 | 30 | 99.7 | 200 |
| 9E-30 | 6.0 | 0.409 | 21 | 30 | 99.7 | 400 |

**Table 4**

Platinum sputter coating polymer membrane in contact with solution electrical current parameters, 0.7mA Current

| Sample # | Platinum Coating Thickness (nm) | Solution Volume (mL) | Solution Temperature (°C) | Applied Electrical Current (mA) | Solution Acetic Acid % (vol%) | # Current Cycles |
|---|---|---|---|---|---|---|
| 1E-07 | 6.0 | 0.409 | 21 | 0.7 | 5 | 100 |
| 2E-07 | 6.0 | 0.409 | 21 | 0.7 | 5 | 200 |
| 3E-07 | 6.0 | 0.409 | 21 | 0.7 | 5 | 400 |

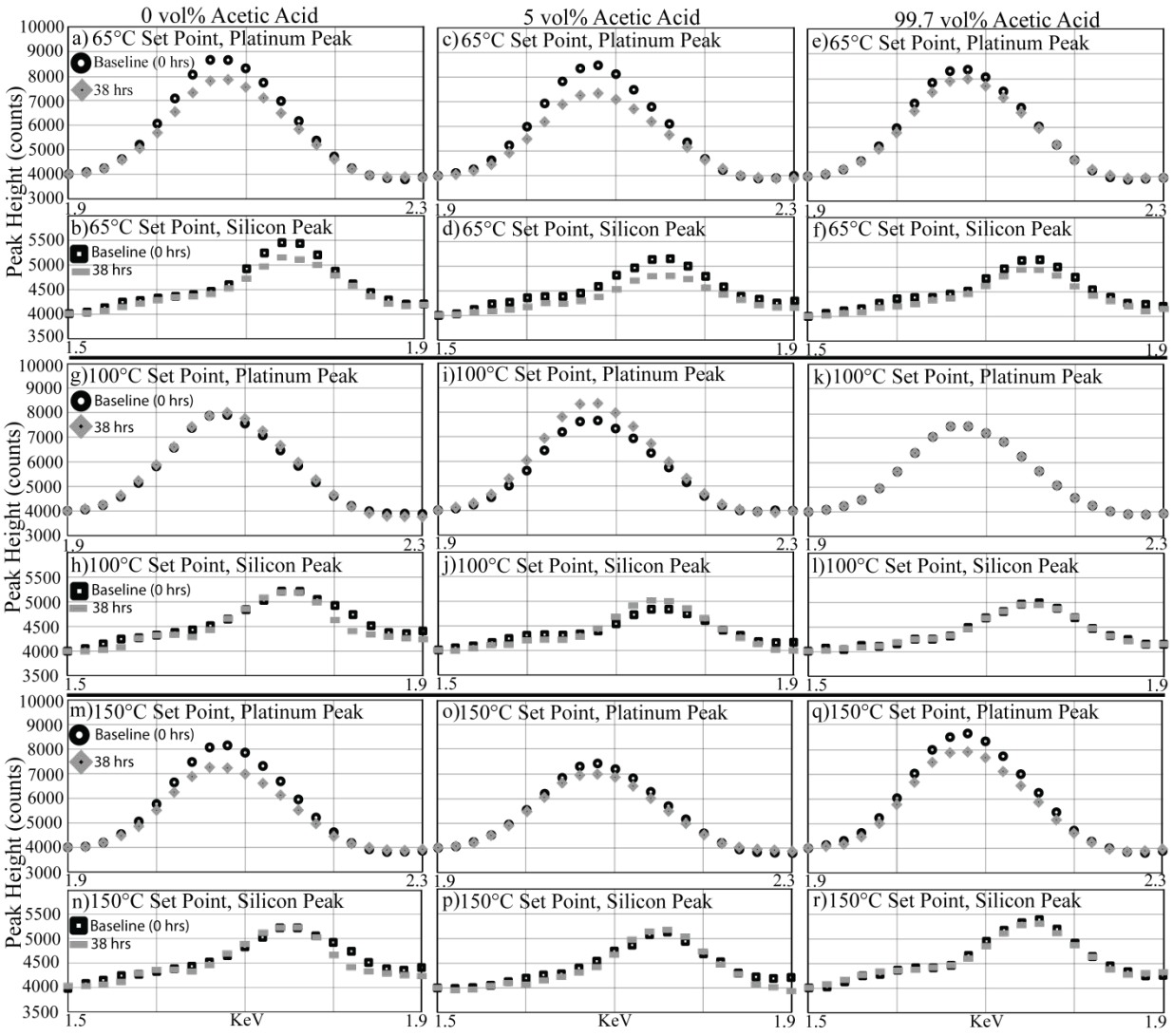


**Fig. 2.** EDS spectrums of platinum sputter-coated polymer membranes heated using a (a-f) 65°C, (g-l) 100°C and (m-r) 150°C set point at atmospheric pressure for 38hrs. Platinum coated polymer membranes were submerged in (a,b,g,h,m,n) 0 vol% acetic acid, (c,d,l,j,o,p) 5 vol% acetic acid and (e,f,k,l,q,r) 99.7 vol% acetic acid for 38hrs. Baseline (before heating occurred) platinum ( ⭘ ) and silicon ( ◘ ) data are shown along with platinum (◆) and (▬) silicon data after being heated 38 hrs. All data collected before and after have been adjusted so they start near the same initial value.

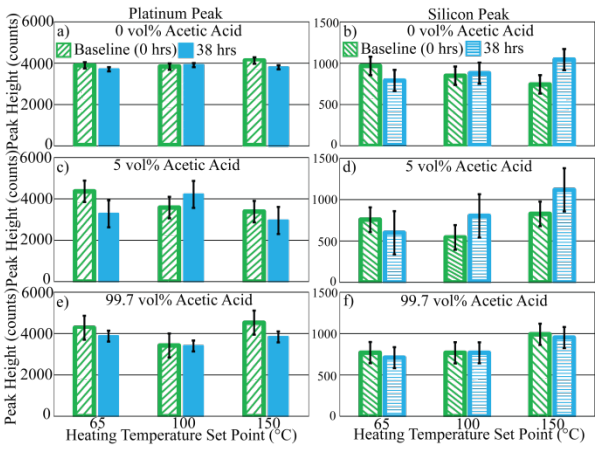


**Fig. 3.** The average EDS values for platinum and silicon peaks from polymer membranes submerged in (a-b) 0 vol% solution, (c-d) 5 vol% solution and (e-f) 99.7 vol% solution while being heated at 65°C, 100°C and 150°C set points at atmospheric pressure. Average EDS baseline (before heating occurred) platinum (▨) and silicon (▧) data are shown along with average platinum (■) and silicon (▤) EDS data after being heated using 65°C, 100°C and 150°C set points for 38 hrs. Three sets of data were used for each parameter average and standard deviation reported.

Fig. 4 shows XRD spectra from samples before and after being heated using a 65°C, 100°C and 150°C set point. Two peaks were detected and identified as the (0,1,1) and (0,2,2) quartz peaks located at 26.9° and 55.6° Two-Theta, respectively. Fig. 4(a-c) shows the polymer quartz peak intensity when heated, submerged in either (a) 0 vol%, (b) 5 vol% or (c) 99.7 vol% acetic acid drastically increased compared to the baseline spectra which was unheated polymer material. The two peaks maintain the same Two-Theta position for all heating experiments.

Fig. 5 shows the particle size and strain data calculated using the Williamson-Hall method [35] from the XRD spectra in Fig. 4. Fig. 5(a) shows the particle size of the quartz did not statistically change compared to the baseline sample when heated and submerged in the different solutions while Fig. 5(b) shows the lattice strain did not change compared to the baseline when heated and submerged in the different solutions.

While the strain on the quartz lattice structure did not statistically change compared to the initial baseline the strain did, on average, decrease, which may be the result of the quartz being arranged in a more preferred orientation to minimize strain while being heated. A more preferred quartz particle orientation could possibly have increased the XRD peak intensity.

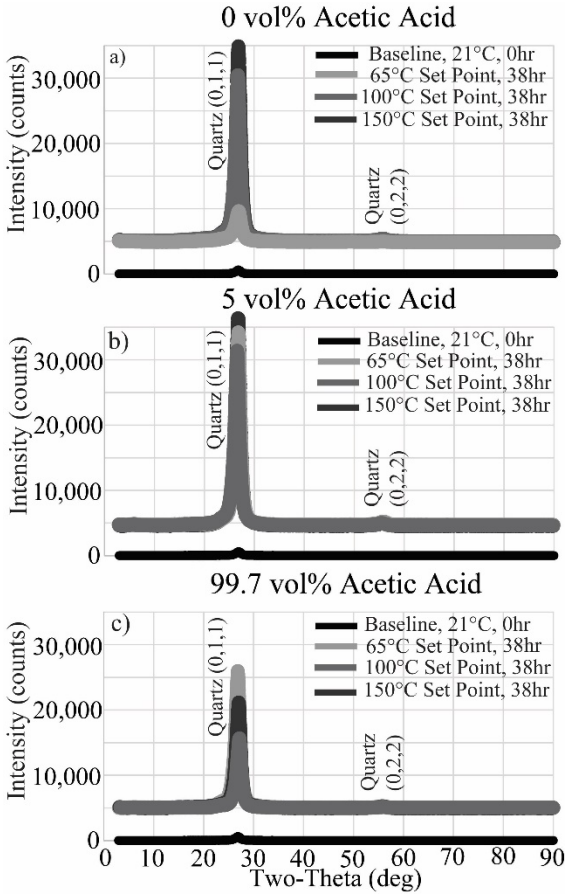


**Fig. 4**. XRD spectra for baseline (before heating occurred) polymer samples and samples heated using 65°C, 100°C and 150°C set points at atmospheric pressure submerged in (a) 0 vol% acetic acid, (b) 5 vol% acetic acid and (c) 99.7 vol% acetic acid. Quartz peaks were located at ~26.9° and 55.7° Two-Theta. The quartz reference spectrum came from the ICSD database # 71393 [36].

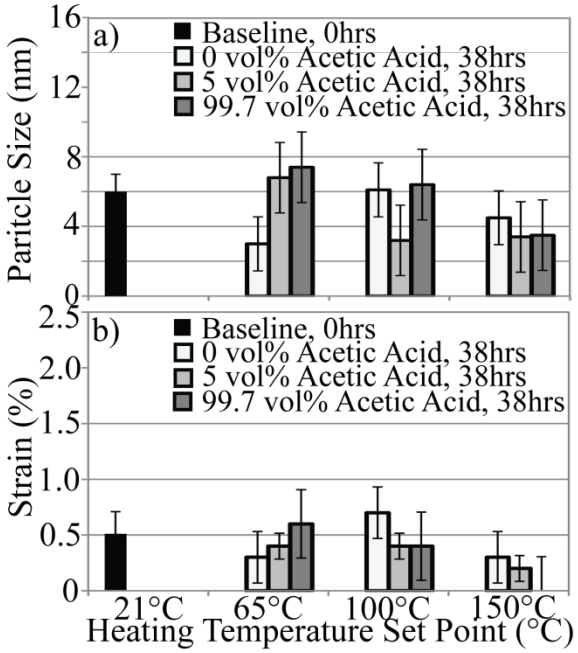


**Fig. 5.** Williamson-Hall quartz (a) particle size and (b) strain data calculated using XRD spectra from baseline (before heating occurred) polymer membrane samples and samples heating using 65°C, 100°C and 150°C set points at atmospheric pressure submerged in 0 vol%, 5 vol% and 99.7 vol% acetic acid.

### *3.2 The effect of electrical current and solution acidity concentration on platinum and silicon particle levels*

Platinum sputter-coated polymer membrane samples next had an electrical current applied to test whether the flow of electrons through the electrocatalyst in combination with different solution chemistries could result in platinum being removed.

Fig. 6 shows platinum and silicon EDS peak intensities from the platinum sputter-coated membrane samples before and after having a 30mA current applied using the experimental conditions shown in Table 3. Platinum was statistically decreased by ~38% after 400 cycles while silicon increased in all samples when in contact with 0 vol% acetic acid solution. Platinum showed a near 100% removal with as few as 50 cycles while silicon showed no changes in intensity when in contact with 5 vol% acetic acid. Platinum and silicon both showed no changes in intensity for 50 to 200 cycles when in contact with 99.7 vol% acetic acid.

Fig. 7 shows platinum and silicon EDS peak intensities from the platinum sputter-coated membrane samples before and after having a 0.7mA current applied using the experimental conditions shown in Table 4. The 0 vol% and 99.7 vol% acetic acid solutions were not compared using the 0.7mA curent since the 5 vol% solution showed the most dramatic impact when tested using 30mA, and was considered the most likely to show detectable results when using a significantly lower current. EDS results show the platinum decreased by 36-40% when the 0.7mA current was cycled for 100, 200 and 400 times while silicon did not change for the samples in contact with 5 vol% acetic acid solution. As mentioned previously the voltage through the platinum coating was 2.6V when using the 30mA current, and individual fuel cells do not produce potentials that large. It is important to determine whether similar platinum loss results can be observed as was seen in Fig. 6 (a,b,e,f,k,l) using a current and voltage capable of being produced by individual cells.

Fig. 8 shows the average and statistical variations in platinum and silicon peak heights calculated from the 30mA EDS raw data obtained from the three samples used for each adjusted parameter. Overall the averaged platinum and silicon EDS results follow similar trends shown in Fig. 6 and Fig. 7 even after taking into account the standard deviation of each data set collected.

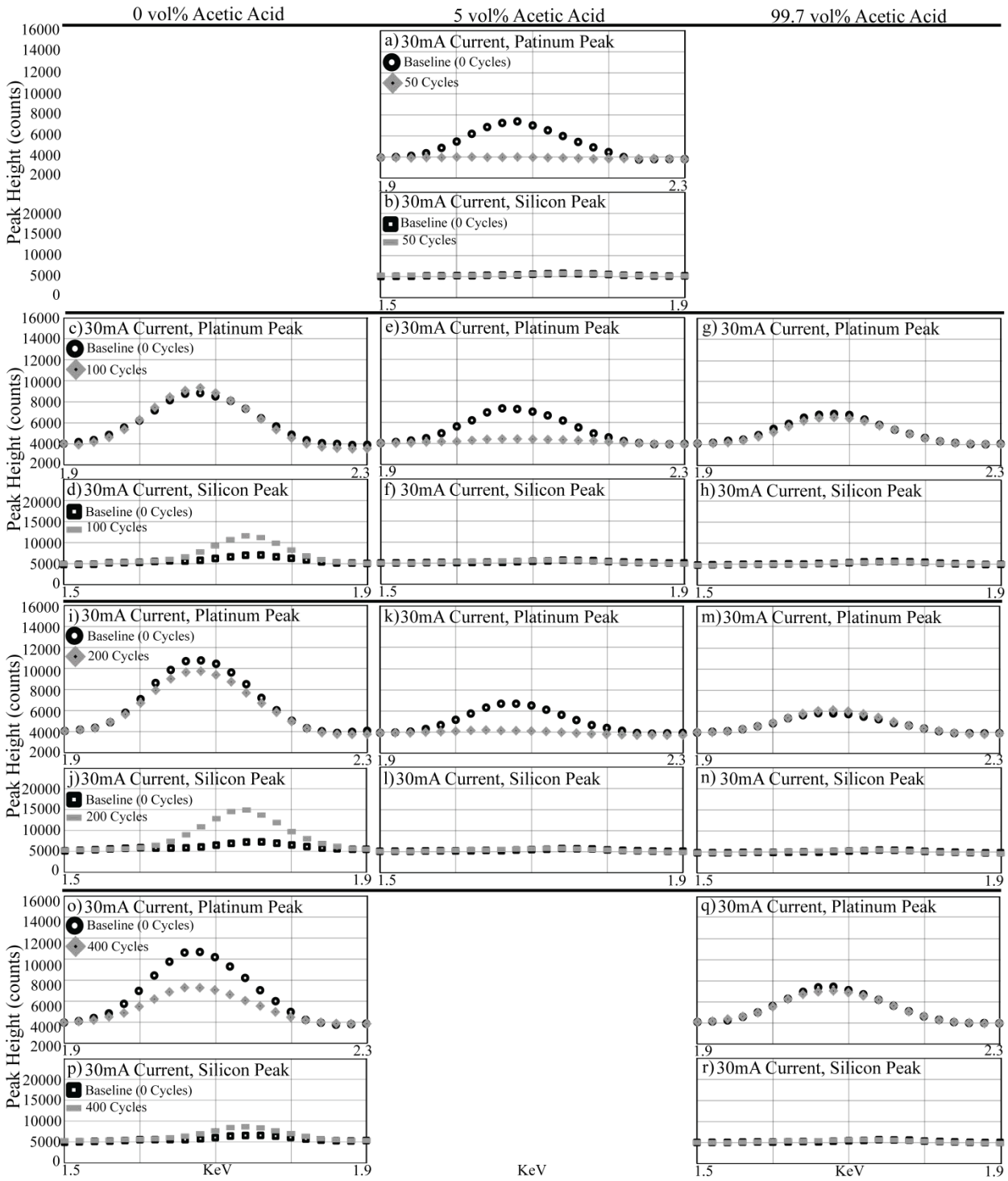


**Fig. 6.** EDS spectrums of platinum sputter-coated polymer membranes applied with a 30mA current applied (a-b) 50 cycles, (c-h) 100 cycles, (i-n) 200 cycles and (o-r) 400 cycles at 21°C. Platinum coated polymer membranes were in contacted with (c,d,l,j,o,p) 0 vol% acetic acid, (a,b,e,f,k,l) 5 vol% acetic acid and (g,h,m,n,q,r) 99.7 vol% acetic acid for either 50, 100, 200 or 400 cycles. Baseline (no current) platinum (●) and silicon (■) data are shown along with platinum (◆) and (▬) silicon data after testing. All data collected before and after have been adjusted so they start near the same initial value.

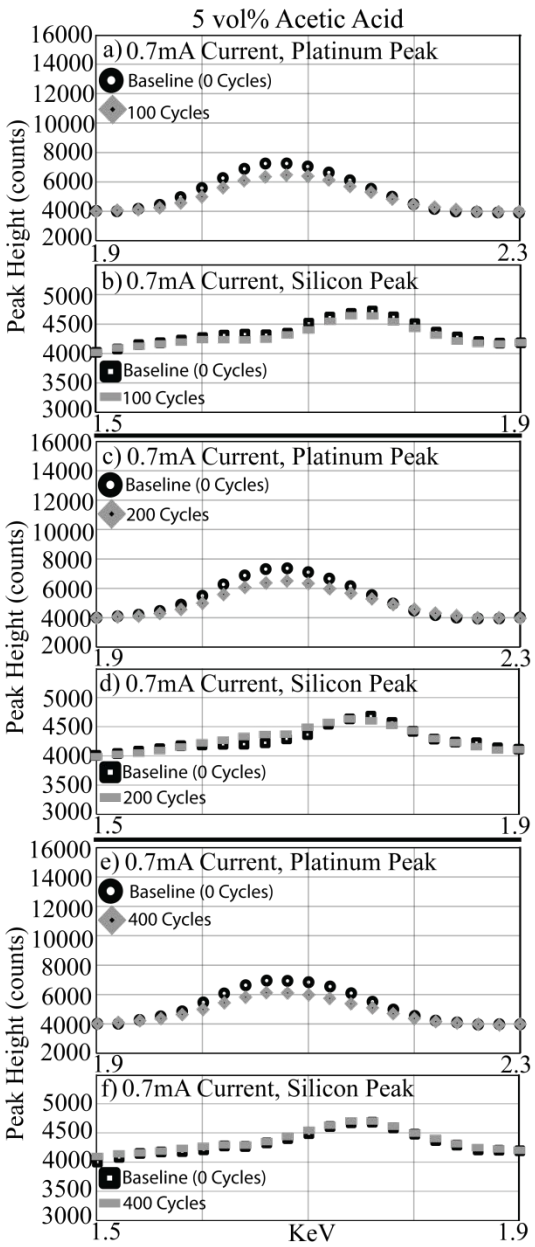


**Fig. 7.** EDS spectrums of platinum sputter-coated polymer membranes applied with a 0.7mA current applied (a-b) 100 cycles, (c-d) 200 cycles and (e-f) 400 cycles at 21°C. All platinum coated polymer membranes were in contacted with 5 vol% acetic acid during testing. Baseline (no current) platinum (●) and silicon (■) data are shown along with platinum (◆) and (▬) silicon data after testing. All data collected before and after have been adjusted so they start near the same initial value.

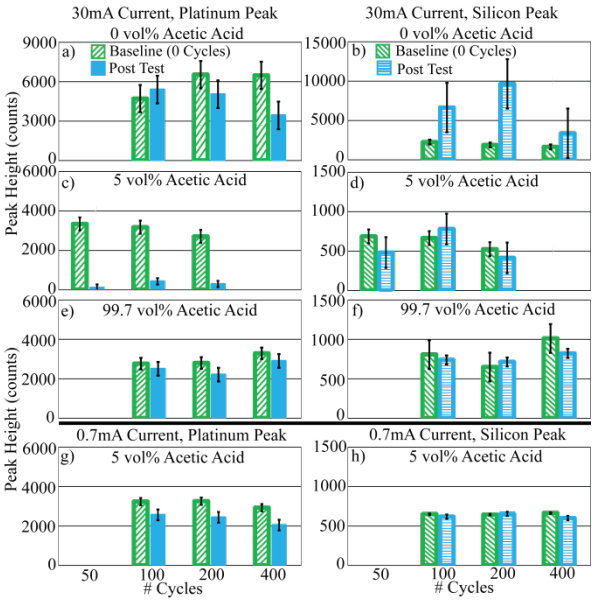


**Fig. 8.** The average EDS values for platinum and silicon peaks from polymer membranes in contact with (a-b) 0 vol% solution, (c-d) 5 vol% solution and (e-f) 99.7 vol% solution while being applied with a 30mA current. Polymer membranes in contact with (g-h) 5 vol% acetic acid also had a 0.7mA current applied. All samples were cycled for 50, 100, 200 and 400 times at 21°C. Average EDS baseline (no current) platinum (▨) and silicon (▨) data are shown along with average platinum (■) and silicon (▤) EDS data after testing. Three sets of data were used for each parameter average and standard deviation reported.

Fig. 9 shows the platinum and silicon EDS peak intensities from the platinum sputter-coated membrane samples before and after having 30mA current applied for 100, 200 and 400 cycles, using no solution and the experimental conditions shown in Table 5. Unlike the previous two raw EDS plots, using different solutions in contact with the platinum coating, both the platinum and silicon levels did not show any change when no solution was present. This suggests that the quartz and/or electrical current are not sufficient to change the platinum and silicon levels.

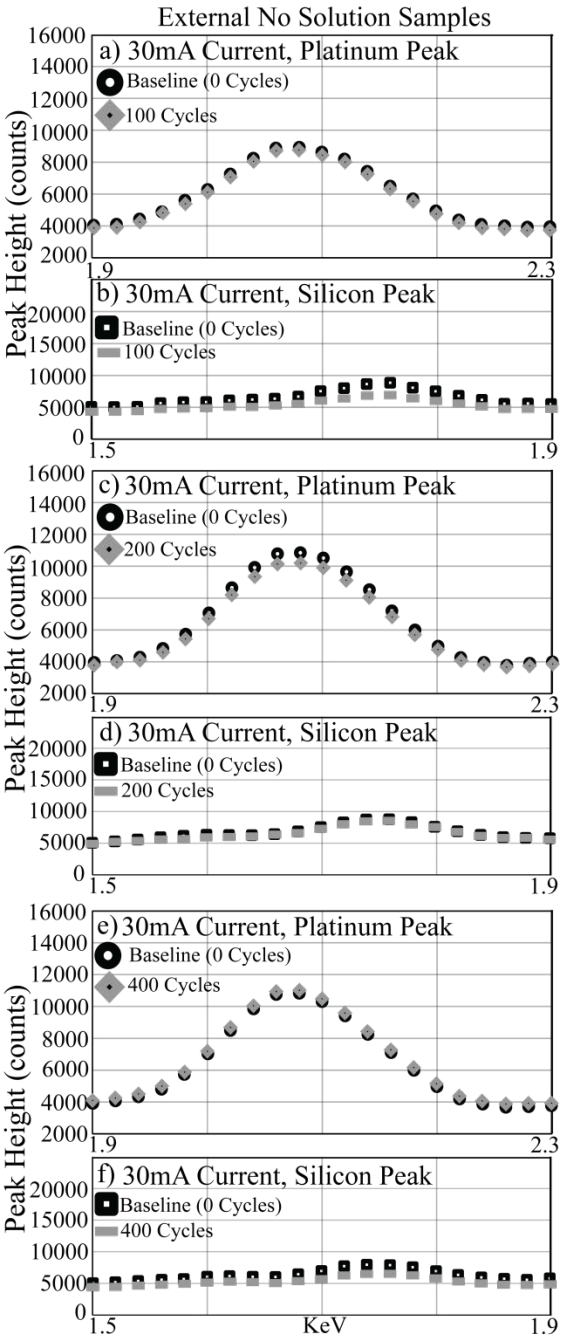


**Fig. 9**: EDS spectrums of platinum sputter-coated polymer membranes applied with a 30mA current applied (a-b) 100 cycles, (c-d) 200 cycles and (e-f) 400 cycles at 21°C. All samples were located outside the solution during testing. Baseline (no current) platinum (●) and silicon (■) data are shown along with platinum (◆) and (▬) silicon data after testing. All data collected before and after have been adjusted so they start near the same initial value.

Fig. 10 shows XRD spectra from samples before and after a 30mA current was applied 50, 100, 200 and 400 times at 21°C in contact with (a) 0 vol%, (b) 5 vol% and (c) 99.7 vol% acetic acid solutions. Fig. 10(a-c) shows the polymer quartz peak intensity increased compared to the baseline spectra which was unheated polymer material, but did not increase to nearly the same magnitude as the heated samples shown in Fig. 4. The two quartz peaks maintained the same Two-Theta position for all cycle experiments.

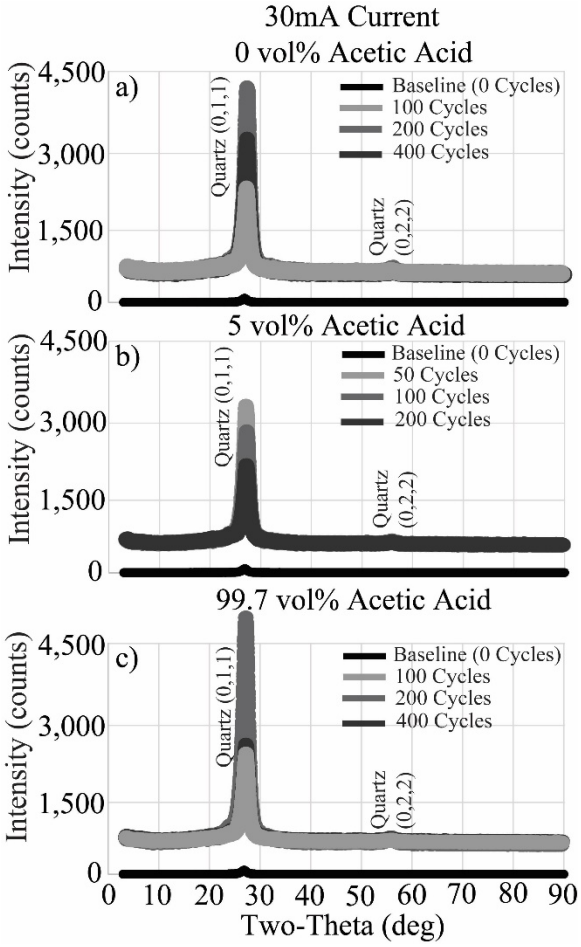


**Fig. 10.** XRD spectra for baseline (no current) polymer samples and samples tested using a 30mA for 50, 100, 200, and 400 cycles at 21°C in contact with (a) 0 vol% acetic acid, (b) 5 vol% acetic acid and (c) 99.7 vol% acetic acid. Quartz peaks were located at ~26.9° and 55.7° Two-Theta. The quartz reference spectrum came from the ICSD database # 71393 [36].

**Table 5**
Platinum sputter coating polymer membrane external to solution electrical current parameters

| Sample # | Platinum Coating Thickness (nm) | Solution Volume (mL) | Solution Temperature (°C) | Applied Electrical Current (mA) | Solution Acetic Acid % (vol%) | # Current Cycles |
|---|---|---|---|---|---|---|
| 1NS | 6.0 | 0.409 | 21 | 30 | No Solution | 100 |
| 2NS | 6.0 | 0.409 | 21 | 30 | No Solution | 200 |
| 3NS | 6.0 | 0.409 | 21 | 30 | No Solution | 400 |

Fig. 11 shows XRD spectra from samples before and after a 0.7mA current was applied 100, 200 and 400 cycles at 21°C in contact with 5 vol% acetic acid. Similar to the 30mA XRD results the quartz peak intensity increased when compared to the baseline spectra. While the peak intensity values did not increase as significantly as the 30mA samples, their average intensity was still 82% of average results in Fig. 10 and is considered similar. The two quartz peaks maintained the same Two-Theta position for all cycle experiments.

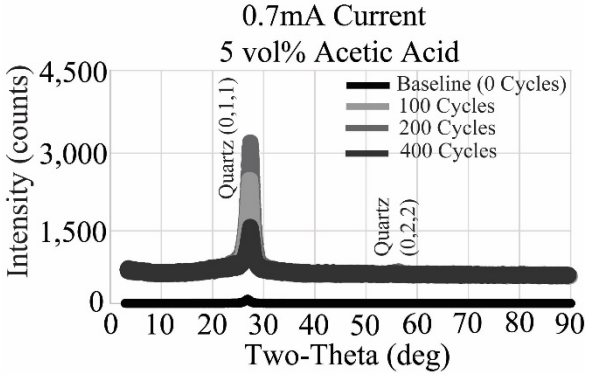


**Fig. 11.** XRD spectra for baseline (no current) polymer samples and samples tested using a 0.7mA for 100, 200, and 400 cycles at 21°C in contact with 5 vol% acetic acid. Quartz peaks were located at ~26.9° and 55.7° Two-Theta. The quartz reference spectrum came from the ICSD database # 71393 [36].

Fig. 12 shows the calculated Williamson-Hall particle size and strain data from the XRD spectra in Fig. 10 and Fig. 11. Fig. 12(a,c) shows the particle size of quartz increased, when compared to the baseline, for samples in contact with 0 vol% acetic acid (30mA current) and 5vol% acetic acid solutions (30mA and 0.7mA currents). The particle size did not change for samples in contact with 99.7 vol% (30mA current) acetic acid solutions. Strain values for all 0.7mA and 30mA samples increased when in contact with either 0 vol% or 5 vol% acetic acid and remained constant when in contact with 99.7 vol% acetic acid solutions.

## 4. Discussion

As demonstrated earlier in this paper, elemental platinum had been removed from polymer membrane surfaces after samples had either a 0.7mA or 30mA current applied through the coating while, primarily, in contact with a 5 vol% acetic acid solution. As platinum, quartz and other additives are potentially used in the construction of PEM fuel cells, it is possible that the results shown in this paper could occur during commercial fuel cell operation and degrade stack performance.

The underlying mechanism behind the loss of platinum will be discussed and an explanation for this process be proposed. The following are viewed as possible explanations behind the results shown (based the collected data), which now will be evaluated:

1. The application of a current through the platinum coating resulted in Joule heating (heating which occurs from the passage of an electric current through a conductor) [37] increasing the quartz particle size and lattice strain resulting in platinum being dislodged from the sample surface.
2. Electrolysis of the acetic acid solution [38, 39], through cycling, produced hydrogen & oxygen gasses which promoted the dissolution of platinum [40-44] into the acetic acid. The solution was promoting the loss of platinum from the polymer surface through platinum dissolving in the acidic solution [1, 43, 44].
3. Solutions with electrical conductivity [45] increased the mobilty of quartz in the polymer membrane, under a applied charge gradient, to remove the platinum.

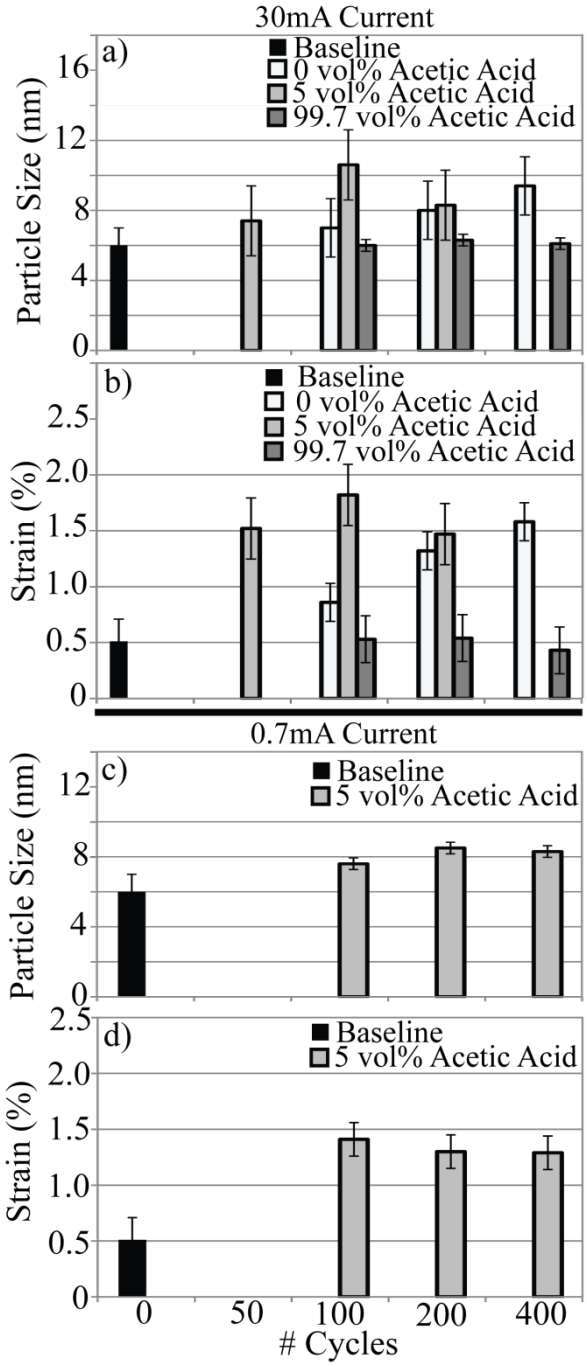


**Fig. 12.** Williamson-Hall quartz (a,c) particle size and (b,c) strain data calculated using XRD spectra 30mA (a-b) and 0.7mA (c-d) currents at 21°C. Baseline (no current) polymer membrane samples and samples tested using 50, 100, 200 and 400 cycles were in contact with (a-b) 0 vol%, (a-d) 5 vol% and (a-b) 99.7 vol% acetic acid.

In the first mechanism it assumes the flow of electrons through the platinum coating produced enough heat to coarsen the quartz particles inside the polymer untimately resulting in the platinum being dislodged from the surface because the quartz nanoparticles increased their lattice strain, broke free from the polymer and impacted the platinum. The results in this paper do not support this mechanism for the following reasons. First, if Joule heating resulted in platinum loss then some platinum loss should be oberved outside the solutions, but as Fig. 9 showed there was no observable platinum loss when current was applied without a solution present. Another possibiliy is that the heating process needed a more conductive medium, such as DI water or acetic acid, to reach the quartz in the polymer samples as the platinum coating was porous and contain air which acted as an insulator limiting heat conduction to the polymer material. If the mechanism behind platinum loss required Joule heating while in the prescence of a solution to transfer heat and coarsen the quartz particles, then the samples tested using DI water should have shown the largest amount of platinum loss since DI water has a larger thermal conductivity compared to acetic acid [46]. While the 0 vol% and 5 vol% solutions do show the quartz particle sizes coarsened and their lattice strain increased, the 99.7 vol% solution did not show any changes in particle size and strain. Based on this proposed mechanism it should have resulted in quartz coarsening as well since thermal conductivity of the acetic acid-water mixture follows a linear trend and the 99.7 vol% solution still has ~27% of the DI water thermal conductivity.

In the second mechanism it assumes a multi-step process for platinum dissolutionv [40, 41] into the 5 vol% acetic acid solution. Some researchers has shown platinum dissolution could occur through the following reaction processes: 1. Platinum can be dissolved as ions under anodic bias [3, 47], 2. Platinum has been reported to form PtO or $PtO_2$ in the prescence of potentials above 1.15V then the $PtO_2$ is dissolved during under cathodic bias while in contact with protons [3, 48] and, 3. Platinum dissolved under bias then transported and preciptated onto a platinum sink in the presence of hydrogen gas [40]. Hydrogen gas production has been shown by Hicks and Fedkiw [38] to be from Kolby electrolysis when bias voltages of 3V or greater were applied to platinum coated Membrane Electrode Assemblies (MEAs) in contact with gaseous acetic acid. There are a number of differences between these reported reaction mechanisms and what was observed in this paper.

The first difference with this second mechanism is that while applying 30mA of current did generate a

2.6V bias which is above 1.15V, and possibly could result in platintum dissolving as ions in solution, later experiments using 0.7mA current had a 0.06V bias which was well below the 1.15V and still demonstrated 36-40% platinum loss. Zhang *et al.* [41] proposed a variation on this reaction mechanism and stated that the lower potential had an impact on the amount of platinum dissolution that occurred. They used an upper voltage of 1.35V and varied the lower voltage from 0.1V to 1V, for 3000 cycles (approximately 200 min), and found the largest amount of platinum loss occurred using a lower potential of 0.8V. The study conducted in this report used upper voltages of 2.6V (2s) and 0.06V (2s) and a lower voltage of 0V (2s), while a lower voltage of 0V reported minimal platinum loss by Zhang *et al.* [41]. In addition the study in this paper demonstrated catestophic platinum loss after only 50 cycles (approximately 8 min), which is a much faster process than what Zhang *et al.* showed.

Another difference is that for $PtO_2$ to form, and be dissolved, there needs to be an ample supply of oxygen gas available, which is not consistent across all solutions used in this report. Electrolysis of both the 0 vol% and the 5 vol% acetic acid solutions would produce oxygen gas but only when using the 30mA current and in small quantities. Since similar amounts of oxygen should be produced in both the 0 vol% and 5 vol% solutions both solutions would be expected to show similar amounts of platinum loss, which the 30mA tests in this report do not show. The 0.7mA results in this paper would also not be expected to occur through this mechanism since the 0.06V across the coating was too low to cause electrolysis in addition to solutions containing a low oxygen environment.

One last difference with this second mechanism is that Holby *et al.* [40] report platinum dissolution and precipiation in the presence of hydrogen gas, using a 0.95V bias, reported that platinum particle sizes needed to be <2nm for significant degradation to occur, which also is inconsistent with the findings in this study. When an average platinum particle size 5nm or greater was used Holby *et al.* reported the platinum surface area stayed nearly constant during 5,000 hrs of testing. Similar to Zhang *et al.* the process reported by Holby *et al.* is operating on a different time scale than the mechanism observed in this report for platinum loss to occur. The sputter-coated platinum particle size was determined using the Williamson-Hall method after sputter-coating different platinum thicknesses onto low background XRD mounting slides, shown in Fig. 13, since the background noise for previous sample XRD spectra obscured the platinum peaks. Platinum thickness values of 6nm, 10nm, 15nm and 20nm were coated onto the slides which showed the primary (1,1,1) peak at 39.56° Two-Theta, (2,0,0) peak at 45.67° Two-Theta and the (2,2,0) peak at 66.57° Two-Theta. The broad amorphous peak at 24.52° Two-Theta was from the mounting slide. The XRD spectra for 6nm platinum thickness only had one peak, so a particle size could not be determined, but the other three samples had platinum particle sizes between 6-7nm. Even though the 6nm thickness platinum particle size could not be determined it is most likely similar to the other sample thicknesses since coating thickness did not change particle size drastically. Since platinum particle sizes are greater than 5nm this mechanism is concluded to not be the mechanism for platinum loss in this report.

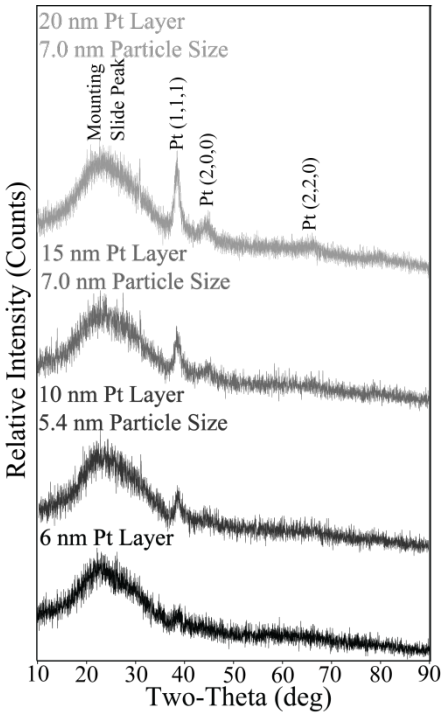


**Fig. 13.** XRD spectra for sputter-coated platinum on low background XRD mounting slides. Platinum sputter-coatings were applied with 6 nm, 10 nm, 15 nm and 20 nm thicknesses. The broad amorphous peak at 24.52° Two-Theta was from the mounting slide. Williamson-Hall determined platinum particle sizes were between 6-7 nm using platinum peaks located at 39.56°, 45.67° and 66.57° Two-Theta. The platinum reference spectrum came from the ICSD database # 41525 [49].

The third mechanism assumes the quartz, in contact with an electrically conductive solution, was transported to the polymer surface and increased its particle size and lattice strain by combining with the platinum to subsequently break from the membrane

from increased lattice strain. Data in this report supports this mechanism for the following reasons. Quartz has been reported in litertaure [50, 51] to be a piezioelectric material where a dipole in the crystal structure is produced when quartz is placed under mechanical strain. Williamson-Hall calculated strain values in Fig. 12 show quartz had 0.5% lattice strain in each sample after fabrication which supports dipoles are present. The application of either a 0.7mA or 30mA current through the coating would create an electrical driving force. This driving force transported the quartz near the polymer surface. The polymer substrate used in this paper, PBI, has already been shown to be cabable of transporting protons [52] in addition to litertaure studies reporting many polymers types have high ionic conductivities overall [53, 54]. The addition of an electronically conduction solution (5 vol% acetic acid) [45, 55], or one that becomes conductive over time (0 vol% acetic acid) [56], to each sample is assumed to increase the magnitude and range of the driving force acting on the quartz nano-particles, which supports the observed increase in silicon levels shown in Fig. 8b. The increased quartz particle size and strain calculated in Fig. 12 are understood to be the result of the quartz interacting with the platinum (either through lattice diffusion or surface bonding), increasing the particle size and strain and dislodging the quartz and platinum simultaneously. Silicon levels in Fig. 8d are thought to be lower than Fig. 8b due to quartz and platinum being removed at such a fast rate due to the increased solution conductivity.

## 5. Conclusions

In conclusion, the platinum catalyst was found to be impacted by the conductivity of the solution produced by the PEM fuel cell while an electrical current was applied during operation. The following mechanism was proposed to explain this process along with these key results.

1. A 0.7mA or 30mA electrical current was passed through the platinum coating, while in contact with an electrically conductive solution (5 vol% acetic acid) resulting in platinum being removed. Applying a 0.7mA current removed 36-40% of the platinum across the entire sample, while applying a 30mA current resulted in platinum being removed entirely across samples.
2. The solution conductivity was found to be the primary variable that influenced the increased platinum loss in each sample using either a 0 vol% or 5 vol% acetic acid solution. The 0 vol% acetic acid solution gradually increased its electrical conductivity over time, resulting in gradual increases in platinum loss. The 5 vol% acetic acid was immediately electrically conductive and had higher conductivity which resulted in the largest platinum loss observed.
3. The mechanism understood behind this process, supported by results, involved quartz nano-particles (with stress induced dipoles) being transported to the platinum sputter-coating through an induced electric charge gradient through the platinum. Larger solution conductivity values increase the number of quartz nano-particles that are brought to the polymer surface which can interact with the platinum nano-particles. The attachment of the platinum nano-particles onto the quartz increases its particle size and lattice strain and resulted in quartz-platinum separation from the polymer surface.


## Acknowledgements

The authors thank Demetrios Tzelepis and Ian Toppler for technical assistance and the use of the SEM, EDS and XRD equipment. The authors also thank Dr. Yi Ding for providing helpful discussions.


## References


[1] Y. Shao-Horn, W. Sheng, S. Chen, P.J. Ferreira, E. Holby, D. Morgan, *Top. Catal.,* "Instability of Supported Platinum Nanoparticles in Low-Temperature Fuel Cells", *vol.* 46, (2007), pp. 285-305.

[2] J.A. Gilbert, N.N. Kariuki, X. Wang, A.J. Kropf, K. Yu, D.J. Groom, P.J. Ferreira, D. Morgan, D.J. Myers, *Electrochim. Acta.,* "Pt Catalyst Degradation in Aqueous and Fuel Cell Environments Studied via In-Operando Anomalous Small-Angle X-ray Scattering", *vol.* 173, (2015), pp. 223-234.

[3] X. Wang, R. Kumar, D.J. Myers, *Electrochem. Solid-State Lett.,* "Effect of Voltage on Platinum Dissolution", *vol.* 9, (2006), pp. A225-A227.

[4] J. Wu, X. Z. Yuan, J.J. Martin, H. Wang, J. Zhang, J. Shen, S. Wu, W. Merida, *J. Power Sources,* "A Review of PEM Fuel Cell Durability: Degradation Mechanisms and Mitigation Strategies", *vol.* 184, (2008), pp. 104-119.

[5] W. Bi, T.F. Fuller, *J. Electrochem. Soc.,* "Temperature Effects on PEM Fuel Cells Pt/C Catalyst Degradation", *vol.* 155, (2008), pp. B215-B221.

[6] M. M. Taghiabadi, M. Zhiani, *Int. J. Hydrog. Energy,* "Degradation Analysis of Dead-Ended Anode PEM Fuel Cell at the Low and High Thermal and Pressure Conditions", *vol.* 44, (2019), pp. 4985-4995.

[7] T. Matsuura, J. Chen, J.B. Siegel, A.G. Stefanopoulou, *Int. J. Hydrog. Energy,* "Degradation Phenomena in PEM Fuel Cell with Dead-Ended Anode", *vol.* 38, (2013), pp. 11346-11356.

[8] S. Strahl, N. Gasamans, J. Llorca, A. Husar, *Int. J. Hydrog. Energy,* "Experimental Analysis of a Degraded Open-Cathode PEM Fuel Cell Stack", *vol.* 39, (2014), pp. 5378-5387.

[9] R. Kerr, H.R. García, M. Rastedt, P. Wagner, S.M. Alfaro, M.T. Romero, C. Terkelsen, T. Steenberg, H.A. Hjuler, *Int. J. Hydrog. Energy,* "Lifetime and Degradation of High Temperature PEM Membrane Electrode Assemblies", *vol.* 40, (2015), pp. 16860-16866.

[10] S. Lang, T.J. Kazdal, F. Kühl, M.J. Hampe, *Int. J. Hydrog. Energy,* "Experimental Investigation and Numerical Simulation of the Electrolyte Loss in a HT-PEM Fuel Cell", *vol.* 40, (2015), pp. 1163-1172.

[11] S.O. Mert, I. Dincer, Z. Ozcelik, *J. Power Sources,* "Exergoeconomic Analysis of a Vehicular PEM Fuel Cell System", *vol.* 165, (2007), pp. 244-252.

[12] W. Bi, Q. Sun, Y. Deng, T.F. Fuller, *Electrochim. Acta.,* "The Effect of Humidity and Oxygen Partial Pressure on Degradation of Pt/C Catalyst in PEM Fuel Cell", *vol.* 54, (2009), pp. 1826-1833.

[13] T. Søndergaard, L.N. Cleemann, L. Zhong, H. Becker, T. Steenberg, H.A. Hijuler, L. Seerup, Q. Li, J.O. Jensen, *Electrocatalysis,* "Catalysis Degradation Under Potential Cycling as an Accelerated Stress Test for PBI-Based High-Temperature PEM Fuel Cells - Effect of Humidification ", *vol.* 9, (2018), pp. 302-313.

[14] M.A. Rubio, A. Urquia, S. Dormido, *Int. J. Hydrog. Energy,* "Diagnosis of Performance Degradation Phenomena in PEM Fuel Cells", *vol.* 35, (2010), pp. 2586-2590.

[15] F. Wang, D. Yang, B. Li, H. Zhang, C. Hao, F. Chang, J. Ma, *Int. J. Hydrog. Energy,* "Investigation of the Recoverable Degradation of PEM Fuel Cell Operated under Drive Cycle and Different Humidities", *vol.* 39, (2014), pp. 14441-14447.

[16] M. Chandesris, R. Vincent, L. Guetza, J.-S. Roch, D. Thoby, M. Quinaud, *Int. J. Hydrog. Energy,* "Membrane Degradation in PEM Fuel Cells: From Experimental Results to Semi-Empirical Degradation Laws", *vol.* 42, (2017), pp. 8139-8149.

[17] J. Kang, J. Kim, *Int. J. Hydrog. Energy,* "Membrane Electrode Assembly Degradation by Dry/Wet Gas on a PEM Fuel Cell", *vol.* 35, (2010), pp. 13125-13130.

[18] D.H. Jeon, K.N. Kim, S.M. Baek, J.H. Nam, *Int. J. Hydrog. Energy,* "The Effect of Relative Humidity of the Cathode on the Performance and the Uniformity of PEM Fuel Cells", *vol.* 36, (2011), pp. 12499-12511.

[19] T. Mittermeier, A, Weiß, F. Hasché, G. Hübner, H.A. Gasteiger, *J. Electrochem. Soc.,* "PEM Fuel Cell Start-Up/Shut-Down Losses vs. Temperature for Non-Graphitized and Graphitized Cathode Carbon Supports", *vol.* 164, (2017), pp. F127-F137.

[20] R.A. Silva, T. Hashimoto, G.E. Thompson, C.M Rangel, *Int. J. Hydrog. Energy,* "Characterization of MEA Degradation for an Open Air Cathode PEM Fuel Cell", *vol.* 37, (2012), pp. 7299-7308.

[21] R. Lin, B. Li, Y.P Hou, J.M. Ma, *Int. J. Hydrog. Energy,* "Investigation of Dynamic Driving Cycle Effect on Performance Degradation and Micro-Structure Change of PEM Fuel Cell", *vol.* 34, (2009), pp. 2369-2376.

[22] E.S. Şayin, A. Bayrakçeken, I. Eroğlu, *Int. J. Hydrog. Energy,* "Durability of PEM Fuel Cell Electrocatalyst Prepared by Microwave Irradiation Technique", *vol.* 37, (2012), pp. 16663-16672.

[23] K. Yu, D.J. Groom, X. Wang, Z. Yang, M. Gummalla, S.C. Ball, D.J. Myers, P.J. Ferreira, *Chem. Mater.,* "Degradation Mechanisms of Platinum Nanoparticle Catalysts in Proton Exchange Membrane Fuel Cells: The Role of Particle Size", *vol.* 26, (2014), pp. 5540-5548.

[24] K. Wang, S. McDermid, J. Li, N. Kremliakova, P. Kozak, C. Song, Y. Tang, J. Zhang, J. Zhang, *J. Power Sources,* "Preparation and Performance of Nano Silica/Nafion Composite Membrane for Proton Exchange Membrane Fuel Cells", *vol.* 184, (2008), pp. 99-103.

[25] Y. Devrim, S. Erkan, N. Baç, I. Eroglu, *Int. J. Energy Res.,* "Nafion/Titanium Silicon Oxide Nanocomposite Membranes for PEM Fuel Cells", *vol.* 37, (2013), pp. 435-442.

[26] Y. Devrim, H. Devrim, *Int. J. Hydrog. Energy,* "PEM Fuel Cell Short Stack Performances of Silica Doped Nanocomposite Membranes", *vol.* 40, (2015), pp. 7870-7878.

[27] C. Lin, T. Haolin, P. Mu, *Int. J. Hydrog. Energy,* "Periodic Nafion-Silica-Heteropolyacids Electrolyte for PEM Fuel Cell Operated near 200°C", *vol.* 37, (2012), pp. 4694-4698.

[28] L. Unnikrishnan, S. Mohanty, S.K. Nayak, *High Perform. Polym.,* "Proton Exchange Membranes from Sulfonated Poly(ether ether keytone) Reinforced with Silica Nanoparticles", *vol.* 25, (2013), pp. 854-867.

[29] N. Zhao, Z. Xie, Z. Shi, *J. Electrochem. En. Conv. Stor.,* "Understanding of Nafion Membrane Additive Behaviors in Proton Exchange Membrane Fuel Cell Conditions", *vol.* 16, (2018), pp.

[30] M.A. Yandrasits, S.J. Hamrock, Membranes for PEM Fuel Cells, Fuel Cell Chemistry and Operation, 2, Amercian Chemical Society, 2010, pp. 15-29.

[31] Y. Shao, J. Liu, Y. Wang, Y. Lin, *J. Mater. Chem.,* "Novel Catalyst Support Materials for PEM Fuel Cells: Current Status and Future Prospects", *vol.* 19, (2009), pp. 46-59.

[32] F.J. Nores-Pondal, I.M.J. Vilella, H. Troiani, M. Granada, S.R. de Miguel, O.A. Scelza, H.R. Corti, *Int. J. Hydrog. Energy,* "Catalytic Activity vs. Size Correlation in Platinum Catalysts of PEM Fuel Cells Prepared on Carbon Black by Different Methods", *vol.* 34, (2009), pp. 8193-8203.

[33] S. Maity, S. Singha, T. Jana, *Polymer,* "Low Acid Leaching PEM for Fuel Cell Based on Polybenzimidazole Nanocomposites with Protic Ionic Liquid Modified Silica", *vol.* 66, (2015), pp. 76-85.

[34] Boyle, J.J., Physics, 4 ed., Prentice Hall College Division, 1995.

[35] V.D. Mote, Y. Purushotham, B.N. Dole, *J. Theor. Appl. Phys.,* "Williamson-Hall Analysis in Estimation of Lattice Strain in Nanometer-Sized ZnO Particles", *vol.* 6, (2012), pp.

[36] J.R. Chelikowsky, N. Troullier, J.L. Martins,H.E. King, *Phys. Rev. B.,* "Pressure Dependence of the Structural Properties of α–Quartz near the Amorphous Transition", *vol.* 44, (1991), pp. 489.

[37] B.V. Balakrishnan, T. Ding, H-P. Phan, D.V. Dao, N-T. Nguyen, *J. Heat Transfer,* "A Generalized Analytical Model for Joule Heating of Segmented Wires", *vol.* 140, (2018), pp. 072001.

[38] M.T. Hicks, P.S. Fedkiw, *J. Electrochem. Soc.,* "Kolbe Electrolysis of Acetic Acid in a Polymer Electrolyte Membrane Reactor", *vol.* 145, (1998), pp. 3728-3734.

[39] N. Ahad, A. de Klerk, *Fuel,* "Fisher-Tropsch Acid Water Processing by Kolbe Electrolysis", *vol.* 211, (2018), pp. 415-419.

[40] E.F. Holbe, W. Sheng, Y. Shao-Horn, D. Morgan, *Energy Environ. Sci.,* "Pt Nanoparticle Stability in PEM Fuel Cells: Influence of Particle Size Distribution and Crossover Hydrogen", *vol.* 2, (2009), pp. 865-871.

[41] H. Zhang, H. Haas, J. Hu, S. Kundu, M. Davis, C. Chuy, *J. Electrochem. Soc.,* "The Impact of Potential Cycling on PEMFC Durability", *vol.* 160, (2013), pp. F840-F847.

[42] S. Mitsushima, Y. Koizumi, S. Uzuka, K-I. Ota, *Electrochim. Acta.,* "Dissolution of Platinum in Acidic Media", *vol.* 54, (2008), pp. 455-460.

[43] S. Cherevko, N. Kulyk, K.J.J. Mayrhofer, *Nano Energy,* "Durability of Platinum-Based Fuel Cell Electrocatalysts: Dissolution of Bulk and Nanoscale Platinum", *vol.* 29, (2016), pp. 275-298.

[44] G. Benke, W. Gnot, *Hydrometallurgy,* "The Electrochemical Dissolution of Platinum", *vol.* 64, (2002), pp. 205-218.

[45] N.F. Hall, H.H. Voge, *J. Am. Chem. Soc.,* "Electrical Conductivities of Mixtures of Sulfuric Acid, Acetic Acid and Water", *vol.* 55, (1933), pp. 239-246.

[46] J.G. Bleazard, T.F. Sun, A.S. Teja, *Int. J. Thermophys.,* "The Thermal Conductivity and Viscosity of Acetic Acid-Water Mixtures", *vol.* 17, (1996), pp. 111-125.

[47] R.M. Darling, J.P. Meyers, *J. Electrochem. Soc.,* "Mathematical Model of Platinum Movement in PEM Fuel Cells", *vol.* 152, (2005), pp. A242-A247.

[48] D.A. Rand, R. Woods, *J. Electroanal. Chem.,* "A Study of the Dissolution of Platinum, Palladium, Rhodium and Gold Electrodes in 1M Sulphuric Acid by Cyclic Voltammetry", *vol.* 35, (1972), pp. 209-218.

[49] J. Häglund, A.F. Guillermet, G. Grimvall, M. Körling, *Phys. Rev. B.,* "Theory of Bonding in Transition-Metal Carbides and Nitrides", *vol.* 48, (1993), pp. 11685.

[50] Uchino, K., Advanced Piezoelectric Materials: Science and Technology, 2 ed., Woodhead Publishing, 2017.

[51] Bechmann, R., *Phys. Rev.,* "Elastic and Piezoelectric Constants of Alpha-Quartz", *vol.* 110, (1958), pp. 1060-1061.

[52] R. Bouchet, E. Siebert, *Solid State Ionics,* "Proton Conduction in Acid Doped Polybenzimidazole", *vol.* 118, (1999), pp. 287-299.

[53] M.A. Ratner, D.F. Shriver, *Chem. Rev.,* "Ion Transport in Solvent-Free Polymers", *vol.* 88, (1988), pp. 109-124.

[54] H.B. Park, C.H. Jung, Y.M. Lee, A.J. Hill, S.J. Pas, S.T. Mudie, E.V. Wagner, B.D. Freeman, D.J. Cookson, *Science,* "Polymers with Cavities Tuned for Fast Selective Transport of Small Molecules and Ions", *vol.* 318, (2007), pp. 254-258.

[55] T.H.C. Salles, C.B. Lombello, M.A. d' Avila, *Materials Research,* "Electrospinning of Gelatin/Poly (Vinyl Pyrrolidone) Blends from Water/Acetic Acid Solutions", *vol.* 18, (2015), pp. 509-518.

[56] R.M. Pashley, M. Rzechowicz, L.R. Pashley, M.J. Francis, *J. Phys. Chem. B.,* "De-Gassed Water is a Better Cleaning Agent", *vol.* 109, (2005), pp. 1231-1238.